J|A|C|S ARTICLES

Published on Web 09/15/2009

# Mapping the Optical Properties of CdSe/CdS Heterostructure Nanocrystals: The Effects of Core Size and Shell Thickness

Joel van Embden,[†] Jacek Jasieniak,[‡] and Paul Mulvaney*

*School of Chemistry and Bio21 Institute, University of Melbourne, Parkville, VIC, 3010, Australia*

Received May 5, 2009; E-mail: mulvaney@unimelb.edu.au

***Abstract:*** Here we present the first comprehensive report on CdSe/CdS heterostructure nanocrystals. The effects of core size and shell thickness on the optical properties of CdSe/CdS heterostructure nanocrystals are investigated. We report a reliable synthetic method to grow thick CdS shells on CdSe cores with sizes ranging from 2.5−4.7 nm. We provide a calibration curve, which enables determination of CdS shell thickness (±0.1 nm) over a wide range of core sizes, circumventing the need for time-consuming HRTEM analyses. Epitaxial growth of the shells was verified by HRTEM, XRD, and SAED. *In-situ* reaction measurements revealed the average per particle (*p*) deposition rates for cadmium and sulfur to be $k_{Cd} = 5.38 \times 10^{-25}$ mol $s^{-1}$ $p^{-1}$ and $k_S = 4.83 \times 10^{-24}$ mol $s^{-1}$ $p^{-1}$. Faster sulfur deposition rates are attributed to the absence of strong sulfur binding ligands in the growth medium. Through the rigorous use of high resolution transmission electron microscopy, a direct link between the dimensions of the heterostructures and their band-edge transition energies, quantum yields, and excited state lifetimes is established. The experiments show that the band-edge transition energies of the core samples, which initially span approximately 431 meV, condense to span only 163 meV after the growth of a 6 monolayer-thick CdS shell. Furthermore, shifts in the band-edge transition energies were found to be extremely sensitive to core size. The QY of the as-prepared core/shells ranged from 25 to 60%. The QYs and band-edge lifetimes of the core/shells were found to depend upon the ligands adsorbed to the particle surface. These data prove that one or both of the charge carriers still has access to the particle surface despite the presence of a 2.2 nm thick CdS shell.

## Introduction

The ability to engineer materials on a nanometer-length scale has sparked interest across many scientific disciplines and has stimulated direct investigation into the fundamental size-dependent properties of matter. Colloidal semiconductor nanocrystals (NCs) have attracted particular attention. It is well known that as-prepared semiconductor nanocrystals exhibit low quantum yields (QY) and that their photoluminescence (PL) is extremely sensitive to the local environment. Although the QY can be increased through passivation of the surface with carefully chosen organic molecules (ligands),[1] these molecules are labile and thus provide no long-term stability. Ligands may desorb from the surface and be replaced by other, less favorable species and they may also undergo side reactions in the solvent.[2] To combat these shortcomings, recent efforts have focused on the development of inorganic surface passivation techniques.[3−8] Epitaxial coating of as-prepared core crystals with a shell of a wider band gap semiconductor provides a means to permanently passivate the core. Shell deposition can, in principle, enable all surface atoms to be passivated, insulating the core from its environment both physically and electronically. Compared to organically passivated cores, core/shell structures can tolerate harsher processing conditions[9] and environments.[10]

It is well-known that the optical properties of core/shell NCs in the strong confinement regime are sensitive to even the smallest changes in core or shell dimensions. As such, the extraction of reliable data on the optical properties of such structures hinges upon unambiguous verification of their physical dimensions through HRTEM investigations. Establishing this link is vital to the credibility of the optical data obtained. Obtaining credible optical information and indeed a comprehensive understanding of any given core/shell system requires that all of the following criteria are fulfilled: (1) The extraction of optical data over a range of core sizes and shell thicknesses; (2) Clear verification of the core and shell dimensions by HRTEM; (3) Adequate structural characterization of the resultant

[†] Current address: Centre for Micro-Photonics, Faculty of Engineering and Industrial Sciences, Swinburne University of Technology, Hawthorn, Victoria 3122, Australia.

[‡] Current address: CSIRO Molecular and Health Technologies, Bayview Ave, Clayton, Victoria 3168, Australia.

(1) Bullen, C.; Mulvaney, P. *Langmuir* **2006**, *22*, 3007.
(2) Liu, H.; Owen, J. S.; Alivisatos, A. P. *J. Am. Chem. Soc.* **2007**, *129*, 305.
(3) Li, J. J.; Wang, Y. A.; Guo, W.; Keay Joel, C.; Mishima Tetsuya, D.; Johnson Matthew, B.; Peng, X. *J. Am. Chem. Soc.* **2003**, *125*, 12567.
(4) Talapin, D. V.; Mekis, I.; Goetzinger, S.; Kornowski, A.; Benson, O.; Weller, H. *J. Phys. Chem. B* **2004**, *108*, 18826.
(5) Steckel, J. S.; Zimmer, J. P.; Coe-Sullivan, S.; Stott, N. E.; Bulovic, V.; Bawendi, M. G. *Angew. Chem., Int. Ed.* **2004**, *43*, 2154.
(6) Fradkin, L.; Langof, L.; Lifshitz, E.; Rogach, A.; Gaponik, N.; Weller, H.; Eychmueller, A. *ChemPhysChem* **2003**, *4*, 1203.
(7) Haubold, S.; Haase, M.; Kornowski, A.; Weller, H. *ChemPhysChem* **2001**, *2*, 331.
(8) Cao, Y.-W.; Banin, U. *Angew. Chem., Int. Ed.* **1999**, *38*, 3692.
(9) Xie, R.; Kolb, U.; Li, J.; Basch, T.; Mews, A. *J. Am. Chem. Soc.* **2005**, *127*, 7480.
(10) Jasieniak, J. J.; Fortunati, I.; Gardin, S.; Signorini, R.; Bozio, R.; Martucci, A.; Mulvaney, P. *Adv. Mater.* **2008**, *20*, 69.

  

particles; (4) Control over shell deposition, yielding of a narrow size distribution throughout shell growth; (5) The growth of spherical core/shell nanocrystals, which removes any ambiguity relating to changes in the optical properties associated with asymmetric shell deposition.

In this article we focus on the synthesis and characterization of CdSe/CdS heterostructure nanocrystals. In spite of the many existing reports on CdSe/CdS nanocrystals,[3,9,11−14] to date there have been no studies that have fulfilled all five of the criteria outlined above. Specifically, most of the existing reports on CdSe/CdS core/shells have not shown sufficient HRTEM in support of their optical data. Reports that have presented adequate HRTEM have focused solely on the production of thick[9] or superthick[14] CdS shells on only a single core size. Other reports have focused on improving the methods of CdS deposition and have been less concerned with optical information.[3,11−13]

Here we present the first comprehensive report on CdSe/CdS heterostructure nanocrystals. A reproducible method to grow cadmium sulfide shells on CdSe nanocrystals of various sizes with submonolayer control of shell thickness is presented. We show, with HRTEM verification, thick CdS shell growth across a range of CdSe core sizes. On the basis of these rigorous HRTEM investigations, we establish a strong link between the core/shell dimensions and their optical response. From these data we present contour plots that permit for the first time the determination of CdS shell thickness to a high degree of accuracy without the need for HRTEM. Via the novel technique of monitoring nanocrystal growth *in situ*, we gather and present valuable information regarding the growth dynamics of the shell. Finally, we map the steady-state and temporal optical properties of the heterostructures as function of their specific dimensions.

## Experimental Section

**Materials.** Cadmium oxide, (99.99%), zinc acetate dihydrate (99.99%), trioctylphosphine (TOP) (90%), 1-octadecene (ODE) (90%), oleic acid (OA) (90%), tributyl phosphite (90%) and sulfur (99.999%) were purchased from Aldrich. Bis(2,2,4-trimethylpentyl)phosphinic acid (TMPPA) was obtained from Cytec Specialty Chemicals. Octadecylamine (ODA) ~95% was procured from Merck. Acetone, chloroform, methanol, ethanol and hexane were all of AR grade and purchased from either Univar or BDH Pty. Ltd. All chemicals and solvents were used without further purification.

**Equipment.** Absorbance measurements were acquired using a Cary 5 UV−vis-NIR spectrophotometer operated in dual beam reference mode. Steady state photoluminescence spectra were taken on a Cary Eclipse fluorescence spectrophotometer. Time resolved photoluminescence measurements were aquired on a Horiba Jobin Yvon Fluorolog-3. High resolution transmission electron microscopy, EDS spectra and electron diffraction were performed using a JEOL 2010 equipped with a Link Si(Li) X-ray detector and a Gatan Image Filter. The instrument was operated at an acceleration voltage of 200 kV. Images were aquired by a slow-scan 2048 × 2048 pixel Gatan CCD camera. X-ray diffraction (XRD) was performed using a Bruker D8 ADVANCE powder diffractometer with a graphite-monochromated copper tube source and scintillation counter detector. *In-situ* time-resolved absorbance measurements were acquired using a custom built high temperature resistant absorbance probe from Ocean Optics. The nanocrystals were illuminated *in situ* from a Mikropak DH-200-BAL deuterium/halogen UV−vis-NIR light source. The spectra were collected by a HR-2000 High-resolution Miniature Fiber Optic Spectrometer in 0.1 s intervals with a 10 ms integration time. Before beginning each experiment a reference spectrum was acquired from a solution consisting of the growth solvent and the precise concentrations of ligands used in the synthetic procedure.

**Injection Solutions.** The cadmium stock solution (0.1 M) was produced by dissolving CdO (0.01 mol, 1.2841 g) in TMPPA (0.04 mol, 11.6 g) and ODE (68.864 g). The solution was first heated to 100 °C and degassed for 15 min followed by three pump/purge cycles and then further heated at 300 °C for 1 h under $N_2$. The solution was then allowed to cool to 100 °C and placed under vacuum for 10 min. The solution was then reheated to 300 °C under $N_2$ for a further 2 h and cooled to room temperature. At this time the solution appeared optically clear. The sulfur stock solution (0.1 M) was prepared by heating sulfur powder in ODE at 120 °C for 2 h. Prior to use, both of these mixtures were heated to 60 °C.

**Monolayer Calculations.** The spherical concentric shell model (CSM) was employed to calculate the amount of shell precursor necessary for the growth of each monolayer.[15] Hereafter, referral to a monolayer (ML) will be taken to mean a thickness equal to half the c-lattice parameter of the bulk semiconductor, 0.337 nm in the case of CdS.

The first injection consisted of enough cadmium to make the particles Cd-rich, calculated by determining the number of surface selenium atoms (outermost 0.17 nm), and then adding enough cadmium to passivate all these sites.[16] The following injections, beginning with sulfur, consisted of equimolar amounts of Cd and S necessary to grow concentric CdS shells 1 ML in thickness. For example, the amounts of the injection solutions for a hypothetical reaction containing CdSe cores (1 $\mu$mol, diameter 3.44 nm) are as follows: To make the particles Cd-rich requires 1.93 mL of Cd stock solution to be injected, followed by 3.61 mL of S and Cd stock solutions for the growth of the first monolayer, 4.89 mL of S and Cd stock solutions for the growth of the second monolayer, then 6.36 mL, 8.02 mL, 9.88 mL and finally 11.94 mL of S and Cd stock solutions for the growth of the third, fourth, fifth and sixth MLs respectively. This method of shell growth is referred to as the Selective Ion Layer Adsorption and Reaction (SILAR) technique, first implemented in colloidal systems by Li et al.[3]

The amounts stated above agree to within 6% of those values obtained from simulations of shell growth for a wurtzite CdS shell on a core of the same crystal phase.[15] It is of importance to note that using the synthetic method outlined here the complete growth of each semiconductor layer was only observed after the introduction of 30% excess cadmium monomer. For clarity the volumes of the injection solutions stated above are for a zero excess of cadmium (such that the calculations may be easily reproduced). However, for all the reactions described here the actual volume of each cadmium injection was increased to achieve a 1.3:1 Cd/S mole ratio. In this way we compensate for the strong solubility of the cadmium monomer in solution, with the extent of shell growth limited by the sulfur content in the growth medium.

**Growth Temperatures.** Table 1 lists the optimized reaction temperatures for the growth of CdSe/CdS nanocrystals for various initial CdSe core sizes. For clarity, the size range of the cores is listed in column one, followed by the wavelength range that corresponds to their first absorption maximum in column two. The growth temperatures are listed in columns three and four where "Temp.1" indicates the temperature required for the growth of the first 2 MLs and "Temp.2" for MLs 3−6.

(11) Pan, D.; Wang, Q.; Jiang, S.; Li, X.; An, L. *Adv. Mater.* **2005**, *17*, 176.
(12) Peng, X. G.; Schlamp, M. C.; Kadavanich, A. V.; Alivisatos, A. P. *J. Am. Chem. Soc.* **1997**, *119*, 7019.
(13) Mekis, I.; Talapin, D. V.; Kornowski, A.; Haase, M.; Weller, H. *J. Phys. Chem. B* **2003**, *107*, 7454.
(14) Mahler, B.; Spinicelli, P.; Buil, S.; Quelin, X.; Hermier, J.-P.; Dubertret, B. *Nat. Mater.* **2008**, *7*, 659.
(15) van Embden, J.; Jasieniak, J.; Gomez, D.; Mulvaney, P.; Giersig, M. *Aust. J. Chem.* **2007**, *60*, 457.
(16) Jasieniak, J.; Mulvaney, P. *J. Am. Chem. Soc.* **2007**, *129*, 2841.

***Table 1.*** Required Reaction Temperatures for the Growth of CdSe/CdS Nanocrystals with Various Core Sizes[a]

| Size range (nm) | $\lambda_{max}$ range (nm) | Temp.1 (°C) | Temp.2 (°C) |
|---|---|---|---|
| 2.2−2.7 | 480−530 | 200[b] | 230 |
| 2.7−3.5 | 530−570 | 230 | 240 |
| 3.5−4.6 | 570−600 | 235 | 240 |
| 4.6−6.2 | 600−630 | 235 | 245 |

[a] Temp.1 is required for the growth of the first 2 MLs and Temp.2 is required for that of MLs 3−6. [b] The special case of this size range requires that the 2nd ML is grown at 215 °C.

**Core Preparation.** CdSe cores of various sizes were produced using the binary ligand size control method outlined elsewhere.[17] The as-prepared cores were purified from their reaction byproduct through multiple chloroform−methanol−acetone (∼ 2:2:1 v/v) extractions. The washed nanocrystals were then dispersed in pure ODE. The solutions were then filtered through 0.22 $\mu$m filters, bubbled with $N_2$ to remove trace amounts of volatile solvents and then stored in the dark for later use. The core sizes and concentrations were determined using the calibration curves of Yu et al.[18]

**Core−Shell Synthesis.** The required amount of CdSe core nanocrystals was added to a three neck round-bottom flask along with a mixture of ODE/ODA in a 2.5:1 ratio by weight to produce a 40 $\mu$M dispersion of nanocrystals in the shell growth solvent. The mixture was then heated to 80 °C under vacuum, pump/purged three times and then further heated to the appropriate shell growth temperature depending on the size of the cores (see Table 1). The calculated amounts of the injection solutions were then added in sequential order beginning with cadmium. Immediately after the injection of any cadmium layer supplements of OA were injected into the reaction mixture in a mole ratio of 20:1 (OA/Cd-Injected). After each injection of monomer the solution was allowed to react for 15 min. Although no major changes to the absorbance spectra were observed after approximately 10 min, additional time was given to ensure the complete growth and annealing of each atomic layer. After the growth of each layer a small aliquot was taken for optical measurements. Following the completion of shell growth all crystals were annealed at 200 °C for 1 h and then cooled to room temperature. The resulting core/shell nanocrystals were then washed using the same procedure employed for the washing of the core nanocrystals. The final washings consisted of several precipitations from chloroform/methanol. The core/shells were then dispersed in hexane and placed in the dark for storage. In cases where long-term storage of the core/shells was required, they were kept in their original growth solutions.

## Results and Discussion

To precisely determine the effects of both core size and shell thickness on the optical properties of the resultant particles, monolayer control of shell thickness must be achieved over a wide range of initial core sizes. Furthermore, the precise core sizes and shell thicknesses must be verified unambiguously through the use of HRTEM. In order to realize these goals, we first synthesized CdSe cores with mean sizes 2.55, 3.40, 3.84, and 4.68 nm. Next, these cores were overcoated with CdS adhering to the optimized conditions outlined in the Experimental section. For clarity and brevity the four different core sizes under investigation will hereafter be referred to as *Samples 1−4*, in order of increasing initial core size.

## Structural Characterization

**Electron Microscopy.** Figure 1 shows the HRTEM images and the corresponding histograms obtained for *Samples 1−4* with various CdS shell thicknesses. The HRTEM images correspond to the core CdSe nanocrystals followed by CdSe/CdS with 2 MLs (approximately 0.84 nm), 4 MLs (approximately 1.52 nm) and 6 MLs (approximately 2.19 nm) of CdS shell respectively. Histograms for the growth of CdS shells on *Samples 1−4* are displayed in the lower panels of Figure 1. Particle sizes were gathered on no less than 150 particles per sample. The recorded sizes were then binned into intervals of 0.1 nm and the resultant histograms fitted to Gaussian distributions using a Levenberg−Marquardt algorithm to extract the mean sizes and standard deviations. For direct comparison, the theoretically predicted mean size of the nanocrystals at each stage during the reaction is plotted alongside its corresponding histogram (dashed line). The error associated with the expected mean size at any point during shell growth is assigned a value of a single lattice plane and is displayed by the shaded areas.[19]

Analysis of the HRTEM images in Figure 1 reveals that throughout the growth process the nanocrystals maintain their initial spherical morphology except in the later stages of shell growth for core sizes larger than 3.40 nm (Panels L and P), where the nanocrystals begin to adopt a distinctly hexagonal shape. Table 2 summarizes the statistics obtained from fitting the histograms to Gaussian functions. Upon inspection of Table 2 it can be seen that in all cases the particle size distributions (PSD) narrow significantly following the growth of the first 2 MLs of CdS (ref: deviation in measured $\bar{d}_m$). The size distributions then broaden slightly with each additional monolayer. The distributions of the final core/shells with 6 MLs of CdS have fwhm typically around 0.1−0.2 nm greater than those of the original cores. Although the fwhm is a better absolute measure of the size distribution, for reference the standard deviations ($\sigma$ (%)) of the distributions are also tabulated. It is seen that in all cases $\sigma$ decreased by ∼2 − 7% by the termination of shell growth and that the final standard deviation of the core/shell nanocrystal diameters is approximately 5%.

By comparing the peaks of the Gaussian functions (mean nanocrystal sizes; $\bar{d}_m$) to their corresponding predicted sizes ($\bar{d}_p$, dashed lines) it is seen that for all stages during shell growth there is good agreement between these two values. The data of Table 2 show that during shell growth the largest deviation of the mean value of any PSD from its predicted size was 0.31 nm, with a large majority of the values falling within 0.2 nm. Considering radial shell growth, all measured shell thicknesses were found to be within 0.16 nm of the mean predicted shell thicknesses (dashed lines), well under the thickness of a single CdS ML (0.337 nm). From the results of Figure 1 and Table 2 it is clear that when adhering to the specific reaction conditions outlined in the Experimental section, and using two acids to manipulate the growth kinetics, submonolayer control of shell thickness may be achieved across a wide range of initial core sizes.

**X-Ray and Electron Diffraction.** To confirm the crystal phase of the CdSe/CdS core/shell nanocrystals both X-ray and electron diffraction were carried out. Figure 2 (upper panel) displays four X-ray powder diffraction (XRD) spectra. Spectrum A was obtained from 3.40 *nm* CdSe cores. Consistent with previous results, the peak positions agree well with those expected for a

(17) van Embden, J. L.; Mulvaney, P. *Langmuir* **2005**, *21*, 10226.
(18) Yu, W. W.; Qu, L.; Guo, W.; Peng, X. *Chem. Mater.* **2003**, *15*, 2854.
(19) The expected mean size of the CdSe core nanocrystals, based on the calibration curve of Yu et al. (ref 18) is noted to have an error of approximately one lattice plane. This error will propagate and affect the calculations of subsequent particle sizes. Thus we may only expect that the mean observed particle size falls within the range of ∼±0.175 nm (one c-lattice plane for CdSe) of the calculated expected size.

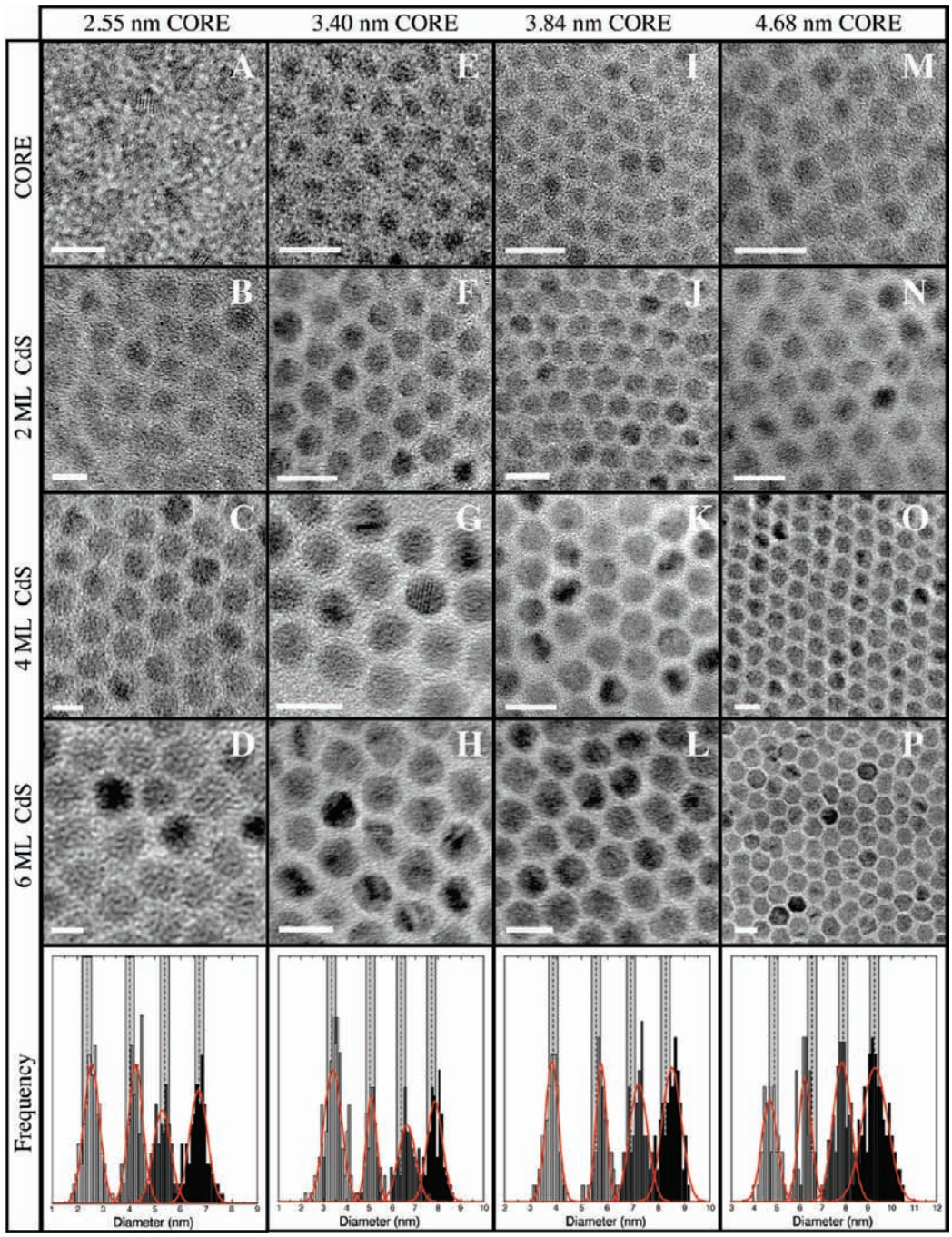


***Figure 1.*** High resolution transmission electron micrographs of CdSe cores with measured diameters of 2.55 nm, 3.40 nm, 3.84 nm and 4.68 nm overcoated with 2 ML, 4 and 6 ML of CdS shell respectively. Scale bar equals 5 nm for Panels A−D and 10 nm for Panels E−P. Histograms of the measured particle sizes obtained during the course of shell growth are displayed in the relevant columns of each initial core size. The dashed line indicates the expected size of the nanocrystals, with the gray box outlining the associated error due to the error in the initial core size calibration curve of Yu et al.[18]

bulk wurtzite CdSe crystal.[20] Spectra B−D were obtained from small (2.55 nm), intermediate (3.40 nm) and large (4.68 nm) CdSe cores with 6 MLs of CdS shell respectively. Upon growth of the shell the peaks sharpen and shift to approach the predicted values for a bulk wurtzite CdS crystal. Both the sharpening and the shifts are consistent with larger local crystal domains and the large volume of CdS compared to CdSe in the final individual structures respectively.[21] Attenuation of the {102} reflection is commonly observed for CdSe and their related heterostructures and arises as a result of zinc blende stacking faults in the {002} direction.[21,22]

Figure 2 (lower panel) displays a selected area electron diffraction pattern (SAED) collected from CdSe/CdS core/shells with a core size of 3.40 *nm* and a 6 ML shell of CdS. The observed relative ring spacings (*d*-spacings) are tabulated along

(20) Jasieniak, J.; Bullen, C.; van Embden, J. L.; Mulvaney, P. *J. Phys. Chem. B* **2005**, *109*, 20665.
(21) Murray, C. B.; Norris, D. J.; Bawendi, M. G. *J. Am. Chem. Soc.* **1993**, *115*, 8706.
(22) Dabbousi, B. O.; Rodriguez-Viejo, J.; Mikulec, F. V.; Heine, J. R.; Mattoussi, H.; Ober, R.; Jensen, K. F.; Bawendi, M. G. *J. Phys. Chem. B* **1997**, *101*, 9463.

***Table 2.*** Statistics Obtained from Analysis of the Histograms Corresponding to the Particle Sizes for *Samples 1−4* at Various Stages of CdS Shell Growth[a]

| sample | CdS ML | energy (eV) | measured $\bar{d}_m$ (nm) | predicted $\bar{d}_p$ (nm) | $(\bar{d}_m - \bar{d}_p)$ (nm) | $\sigma$ (%) |
|---|---|---|---|---|---|---|
| 1 | 0 | 2.477 | 2.55 ± 0.31 | 2.35 | +0.20 | 12.1 |
| 1 | 2 | 2.180 | 4.27 ± 0.29 | 4.03 | +0.24 | 6.7 |
| 1 | 4 | 2.126 | 5.29 ± 0.34 | 5.39 | −0.10 | 6.4 |
| 1 | 6 | 2.124 | 6.71 ± 0.35 | 6.73 | −0.02 | 5.1 |
| 2 | 0 | 2.205 | 3.40 ± 0.38 | 3.32 | +0.08 | 11.2 |
| 2 | 2 | 2.055 | 5.09 ± 0.23 | 5.00 | +0.09 | 4.5 |
| 2 | 4 | 2.027 | 6.64 ± 0.37 | 6.35 | +0.29 | 5.6 |
| 2 | 6 | 2.023 | 7.87 ± 0.33 | 7.70 | +0.17 | 4.3 |
| 3 | 0 | 2.131 | 3.84 ± 0.25 | 3.89 | −0.05 | 6.5 |
| 3 | 2 | 2.030 | 5.77 ± 0.20 | 5.57 | +0.20 | 3.5 |
| 3 | 4 | 2.005 | 7.23 ± 0.35 | 6.92 | +0.31 | 4.8 |
| 3 | 6 | 2.001 | 8.52 ± 0.37 | 8.27 | +0.25 | 4.3 |
| 4 | 0 | 2.046 | 4.68 ± 0.34 | 4.86 | −0.18 | 7.3 |
| 4 | 2 | 1.977 | 6.24 ± 0.28 | 6.55 | −0.31 | 4.5 |
| 4 | 4 | 1.964 | 7.85 ± 0.39 | 7.89 | −0.04 | 5.0 |
| 4 | 6 | 1.961 | 9.29 ± 0.55 | 9.24 | +0.05 | 5.0 |

[a] The energy values listed correspond to the band-edge transition energies of the particles.

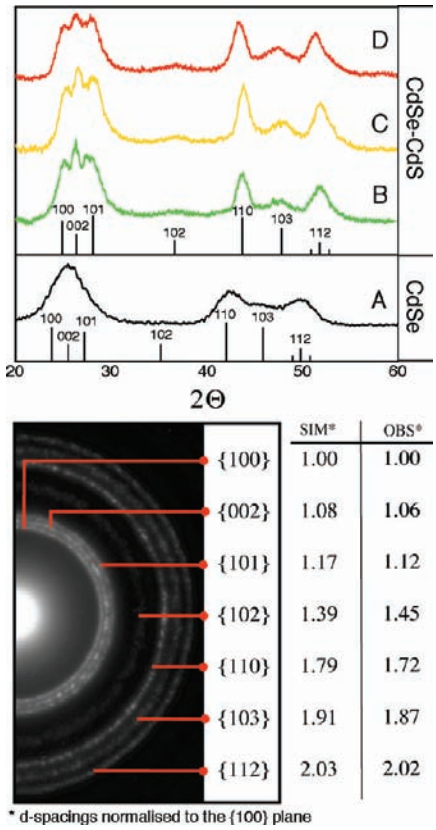


***Figure 2.*** (Upper Panel) Powdered X-ray diffraction patterns of (A) CdSe core, (B−D) CdSe/CdS particles with a 6 ML CdS shell with core sizes 2.55, 3.40 and 4.68 nm respectively. (Lower Panel) Selected area electron diffraction of (C).

with the simulated (SIM) values based on a bulk wurtzite CdS crystal. The OBS and SIM values for each set of Miller indices (hkl values) agree to within 4.6%, which supports the XRD data and confirms the wurtzite crystal phase of the core/shells. Collectively, the data obtained from X-ray and electron diffraction prove that shell growth proceeds in an epitaxial manner.

**HRTEM Structural Analysis.** Figure 3A shows a high resolution transmission electron micrograph of the 2D zone axis of a CdSe/CdS nanocrystal with 6 ML of CdS shell (10.19 nm in diameter, *Sample 4*, Figure 1P). The nanocrystal shown in Panel A is highly crystalline and clearly exhibits hexagonal morphology as well as hexagonal symmetry on the atomic scale. Panel B shows a magnified area of this nanocrystal highlighting the *a* and *c* lattice planes. Panel C shows a simulation of a pure CdS nanocrystal viewed on the same crystal face shown in A and B. The measured and simulated values for the *a* and *c* lattice parameters and $\theta$ are as follows: Measured; $a = 3.941$ Å, $c = 6.823$ Å, $\theta = 60°$. Simulated; $a = 4.135$ Å, $c = 6.749$ Å, $\theta = 60°$. Measured bond distances were obtained by averaging over 20 lattice planes in both directions. Simulated values were obtained from a CdS nanocrystal constructed using bulk CdS lattice parameters and symmetry.[23] From comparison of these values we determine the view direction to be perpendicular to both the {100} plane (*a* axis) and {002} plane (*c* axis). The lattice spacings of the CdSe/CdS heterostructure agree well with those values obtained for a bulk wurtzite CdS nanocrystal. However, a slight contraction of the *a*-lattice parameter (4.7%) and an elongation of the *c* -lattice parameter (5.3%) is observed. This is perhaps a consequence of the small scale of the crystal relative to a bulk crystal or may be due to the strain imposed on the crystal lattice through the core-to-shell lattice mismatch.

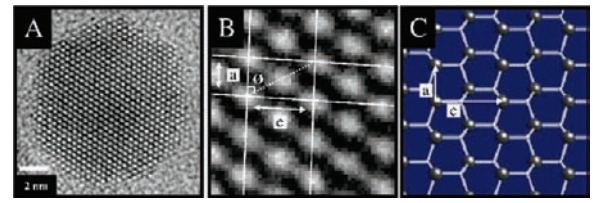


***Figure 3.*** (A) Super high resolution transmission electron micrograph of the 2D zone axis of a CdSe/CdS nanocrystal with 6 ML of CdS shell; 10.19 nm in diameter. Scale bar equals 2 nm. (B) Magnified area of the nanocrystal highlighting the *a* and *c* lattice planes. (C) Simulation of a pure CdS nanocrystal viewed on the same crystal face shown in A and B.

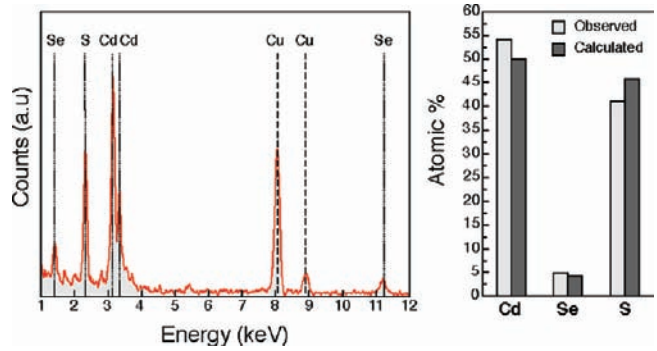


***Figure 4.*** (Left) EDS spectrum of CdSe/CdS nanocrystals with a core size of 3.4 *nm* and a shell thickness of 6 ML. The peaks due to the copper grid are indicated by the dashed lines. (Right) Observed and calculated atomic percentages of Cd, Se and S in the heterostructure.

**Elemental Analysis (EDS).** Figure 4 shows the results of an elemental analysis performed on a selected area of a few hundred CdSe/CdS nanocrystals with a core size of 3.40 nm and 6 ML of CdS shell (See Figure 1 Panel H). The corresponding bar-chart summarizes the observed and calculated relative atomic percentages of cadmium, selenium and sulfur present in each heterostructure. The expected and observed percentages agree to within 4.4% for all three elements analyzed. The close agreement of these values supports the HRTEM sizing data obtained for both the initial core and final particle sizes.

(23) *CrystalMaker 6.3.4*; CrystalMaker Software Limited, 2004.

Furthermore, it rules out the possibility that ripening of the CdSe cores has contributed to the observed shell thickness as in such cases it is expected that (on average) higher amounts of selenium would be present in the final core/shell structures.

## Reaction Conditions

Optimising the conditions for shell growth involves systematically altering a number of reaction variables. The growth medium, temperature, precursor type and concentration as well as the type and amount of free ligand all need to be optimized to achieve the growth of high quality core/shell nanocrystals. Here we report on the most critical parameters, namely the nature of the ligands and the reaction temperature. The effects of the remaining parameters are discussed elsewhere.[15]

**Ligand Chemistry.** The choice of ligand chemistry is perhaps the most vital consideration, because the rate and extent to which monomers are consumed during (shell) growth is reaction controlled by the ligands. The role of the ligands is to balance the particle/monomer reactivity in order to avoid the extremes of ripening or homogeneous nucleation (HN).

Early trials using the precursors Cd-TMPPA and ODES (where TMPPA is the dominant active ligand) to grow a CdS shell were unsuccessful. The shell thicknesses of the resulting core/shells were smaller than predicted and HRTEM investigations revealed the final particles to be highly faceted (see Supporting Information). Furthermore, during these preparations CdS nuclei would invariably appear after 5−6 atomic monolayers (2−3 MLs CdS) had been injected. The formation of these nuclei is signaled by a noticeable decrease in the PL of the core/shells and the formation of strong absorbance and PL bands centered around 400 *nm*, consistent with the formation of isolated CdS nanocrystals. Reactions which included higher concentrations of free TMPPA (up to 1 M) in the injection solution were unable to suppress the formation of these nuclei. Given that we consistently observed HN after 5−6 injections of precursor (specifically after the injection of sulfur monomer) we submit that the formation of isolated CdS is a direct consequence of TMPPA binding strongly to the particle surface, inhibiting shell growth and subsequently causing a build-up of unreacted Cd-TMPPA in solution, which may later nucleate in the presence of sulfur.

In an effort to improve shell growth and prevent HN another cadmium precursor, cadmium oleate, was also trialled. It was found that by employing cadmium oleate with OA/Cd ratios above 10:1, thicker shells could be grown with a reduction in the amount of HN. However, HRTEM images of the core/shells grown using this precursor revealed pronounced growth of the shell along the {002} axis when the CdS shell thicknesses exceeded 4 MLs (see Supporting Information), a result that is consistent with the findings of Li et al.[3] A further drawback of cadmium oleate is that it must be introduced into the growth medium with at least a 10-fold excess of oleic acid in order to adequately suppress HN. While the introduction of this excess acid was found to have a negligible effect on larger core sizes, it caused the dissolution or ripening of those particles with initial sizes below ∼ 3 nm (1st Abs. max. ∼550 nm).

Consistent with previously published data,[17] TMPPA was found to slow growth, inhibit Ostwald ripening and promote HN, while OA facilitated growth and suppressed HN. The opposing effects of these two ligands were used to manipulate the solubility of the monomer as well as particle reactivity in order to provide an environment that was conducive to growth only. After numerous trials it was found that combining these ligands in a mole ratio of 5:1 (OA:TMPPA) provided the conditions necessary for the growth of highly crystalline spherical shells on core sizes ranging from ∼2.2 nm to ∼6.2 nm in the absence of either ripening or HN.

**Reaction Temperature.** The growth rate of a nanocrystal is both size and temperature dependent. Consequently, the temperature at which the nanocrystals are overcoated is critical.[22] To impart maximum crystallinity to the growing shell high temperatures are desirable. High temperatures also increase the reactivity of both the particles and the shell precursors (monomers), which favors shell growth and thereby prevents the build up of monomer in solution—a condition that leads to the homogeneous nucleation of the shell material. Conversely, if the temperature is too high Ostwald ripening of the nanocrystals will occur.

In light of this we found it necessary to tailor the reaction temperature to suit different sized nanocrystals. For example, nanocrystals with sizes above ∼3 nm required initial temperatures greater than 230 °C for shell growth to occur at appreciable rates. However, for cores with sizes less than around 2.7 nm it was found that if the initial reaction temperature exceeded 200 °C ripening of the cores would occur prior to the first injection of shell precursor. Furthermore, in the case of these small cores, if the initial temperature was much below 200 °C, or if the temperature was not suitably raised during the reaction (typically by about 20−30 °C above the initial temperature), large amounts of monomer would remain unreacted in solution, and homogeneous nuclei would eventually appear. It should be noted that the appearance of these nuclei could not be avoided by increasing the time given for each ML to react, even for delays of up to 1 h between subsequent injections. The optimal reaction temperatures for each core size were those that maintained high conversion rates of monomer into shell material throughout the reaction (see Table 1).

Given that high temperatures and high concentrations of cadmium complexing ligands (especially OA) were required to prevent HN, it was imperative to ensure that ripening did not accompany shell growth. Ripening not only broadens the particle size distribution but, if allowed to continue throughout the reaction also results in changes to the absorbance spectra that are unrelated to shell growth, making those values obtained for the absorbance shifts as a function of shell thickness unreliable. As such, during the course of optimisation several trial experiments were undertaken to make certain that the core nanocrystals were stable at their initial growth temperatures and that any later increase in temperature would not trigger ripening of the core/shell nanocrystals. By taking quantitative absorbance spectra over time the size and size distribution of the nanocrystal populations were monitored. If no changes to the spectra were observed the nanocrystal population was regarded as stable. The results of these experiments indicated that the core nanocrystals could be heated at their initial growth temperature for 20−30 min prior to the injection of shell precursor without growth or spectral broadening.[24] Furthermore, without the usual addition of monomer the core/shell nanocrystals could be heated

(24) In the cases where CdSe nanocrystals with diameters below approx. 2.5 nm were used, spectral changes were commonly observed if the cores were heated at their initial temperature for longer than 10 min.

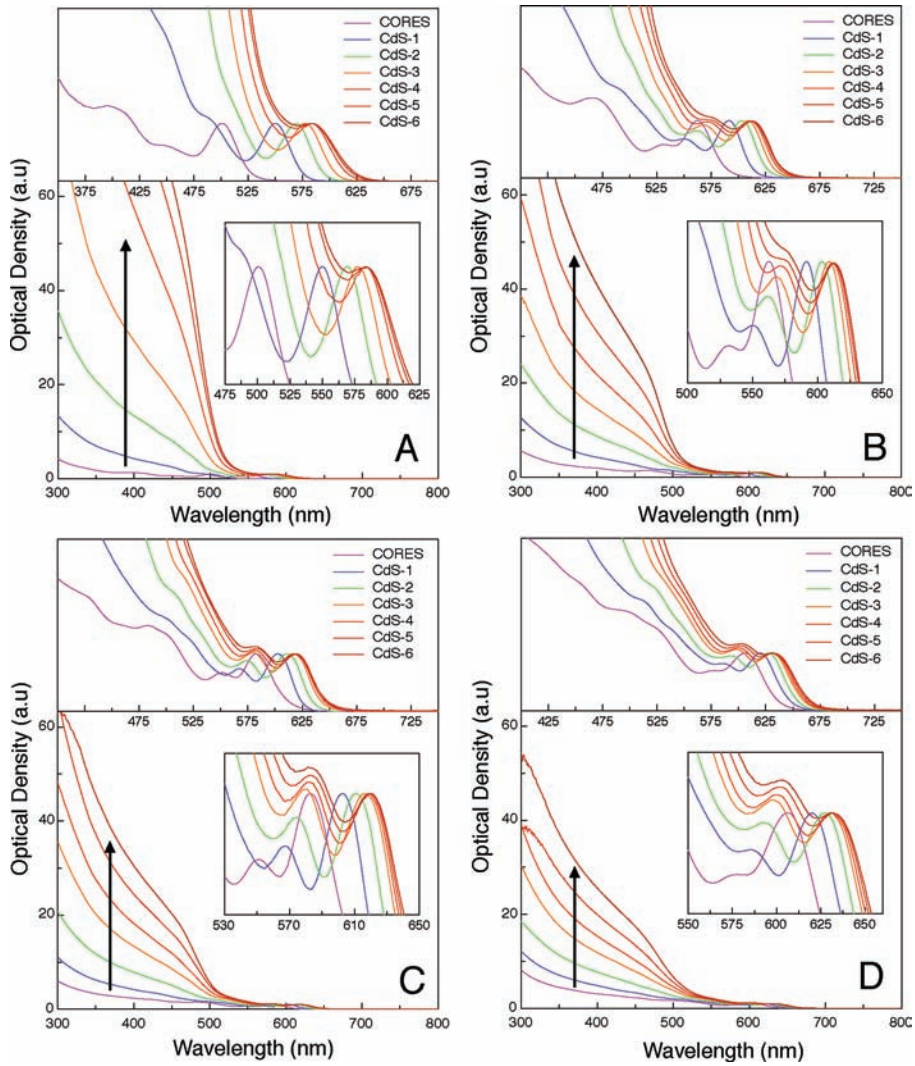


***Figure 5.*** Absorbance spectra as a function of shell thickness for *Samples 1−4* (Panels A−D). For each of these samples the initially narrow band edge transition is maintained throughout shell growth. An increase in absorbance at higher energies is also observed (as indicated by the arrows), which is consistent with the presence of increasing amounts of CdS within the heterostructures.

indefinitely (up to 3 h trialled) following the second temperature increase with no observable changes to the spectra.

## Optical Properties

**Absorbance Shifts.** Figure 5 displays a series of normalized absorbance spectra at different magnifications taken during the growth of a CdS shell on the four samples under investigation. In all four sets of spectra we see that as the CdS shell deposits onto the core a large red-shift of the first excited state occurs. This phenomenon is caused by extensive delocalization of the electron into the surrounding shell and has been previously observed during CdSe/CdS preparations.[3,9] Close examination of the lowest energy $1S_{(h)} - 1S_{(e)}$ transition with increasing shell thickness reveals that the largest red-shift occurs upon deposition of the first monolayer. The magnitude of the shift then declines for each additional monolayer deposited. As the electron delocalizes into the shell its distribution function decays with tunneling distance. Thus as the shell becomes thicker the extent to which the electron may continue to delocalize diminishes. The consequence of this is that the energy of the excited state is most greatly reduced upon the addition of the primary monolayers of the shell. Further inspection of Figure 5 reveals that the second excited state transition ($2S_{(h)} - 1S_{(e)}$) increases in absorption with respect to the band edge transition. This phenomenon is common to CdSe/CdS preparation regardless of the synthetic method used to generate the shell.[3,9,25]

Shell deposition also dramatically increases the absorbance below approximately 500 nm, which is coincident with the onset of the absorption in bulk CdS (approximately 512 nm). As indicated by the arrows, each additional monolayer of CdS that is deposited systematically increases the magnitude of the absorbance at energies below approximately 500 nm. The enormity of these absorbance values relative to the band edge absorbance may be attributed to a combination of the increased absorbance cross-section of the resultant nanostructure, the high shell:core volume ratio, and the high extinction coefficient of CdS compared to CdSe. It should be noted that the absorbance in this spectral region is not due to homogeneous nuclei as indicated by HRTEM investigations. We may also rule out the possibility that the increased absorption is due to reaction byproducts as no changes in absorbance within this region were observed after purification of the particles.

(25) Peng, X.; Schlamp, M. C.; Kadavanich, A. V.; Alivisatos, A. P. *J. Am. Chem. Soc.* **1997**, *119*, 7019.

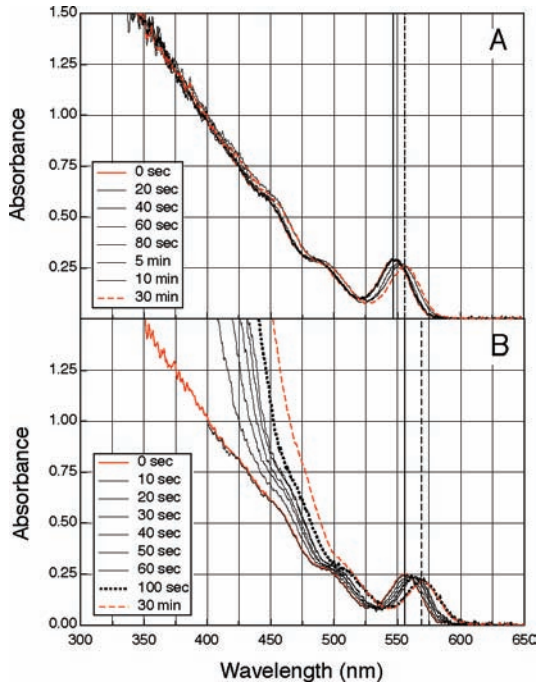


***Figure 6.*** *In-situ* absorbance measurements during CdS shell deposition. (A) Changes to the absorbance spectra after the addition of Cd-TMPPA. (B) Changes to the absorbance spectra after the addition of ODES.

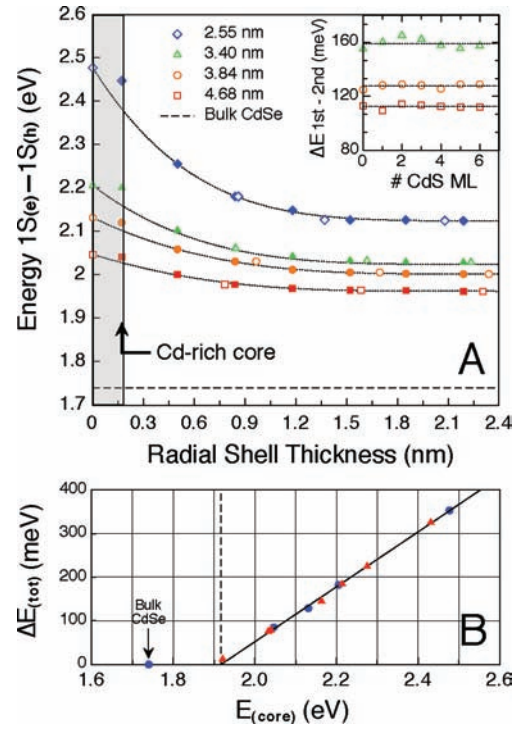


***Figure 7.*** (A) Energy decays of the first excited state, $1S_{(h)} - 1S_{(e)}$, as a function of CdS shell thickness. (B) Total energy loss after CdS shell growth as a function of the initial core energy.

***In-situ*** **Absorption Measurements—Reaction Time Scale.** Figure 6 shows the growth of cadmium and sulfur atomic monolayers at 200 °C monitored by an *in situ* absorbance probe; 2.5 nm CdSe cores were chosen for this experiment as they exhibit the greatest absorbance shifts upon shell deposition. Furthermore, deposition may be conducted at lower temperatures compared to larger cores, which diminishes the extent of spectral broadening due to phonon coupling.[26,27] Panel A shows the spectral changes that occur after the injection of cadmium (2nd Cd-injection) into the reaction solution. No spectral changes were observed in the minute following injection. Between 1 and 10 min the band-edge transition red-shifted 7 nm and a slight increase in the absorbance at higher energies was observed. Continual monitoring of the spectra up to 30 min revealed only a further 1 nm shift with no other changes to the spectral profile observed.

Panel B shows the spectral changes that occur after the injection of sulfur monomer (2nd S-injection). In sharp contrast to the addition of cadmium monomer, the injection of sulfur immediately results in drastic spectral changes. Between 10 and 100 s the band edge transition shifted 14 nm. Each red-shift was accompanied by a concomitant increase in absorbance at higher energies. Between 100 s and 30 min no further red-shifts were observed. However, during this time period an increase in the absorbance within the "shell" spectral region was seen, which may be a sign of increased crystallinity within the particle due to annealing of the lattice.

Comparison of Panels A and B reveals important information about the growth of a CdS shell. First, the red-shift that occurs upon the deposition of cadmium is 40% smaller than the shift due to sulfur. Second, the increase in the absorption at higher energies is almost solely a consequence of sulfur deposition. By comparing the time scales of the two reactions it is clear that cadmium deposition is complete within approximately 10 min and sulfur deposition within 100 s. Using these values, we may calculate the average per particle ($p$) deposition rates. It is found that $k_{Cd} = 5.38 \times 10^{-25}$ mol s$^{-1}$ p$^{-1}$ and $k_S = 4.83 \times 10^{-24}$ mol s$^{-1}$ p$^{-1}$. From these data it is concluded that sulfur deposition occurs at a rate (on average) almost an order of magnitude faster than cadmium. This implies that the activation barrier to the nucleation of monomer at the surface of the particle is largely dependent upon the strength of the ligand-monomer (ligand-particle) bond, with sulfur deposition occurring faster due to the absence of strong sulfur binding additives. Collectively, these results show the strong influence ligands have on the rate of monomer deposition and highlight the importance of precursor choice when tailoring shell growth strategies.

**Transition Energy Changes.** Figure 7A shows the energy shifts of the first excited state ($1S_{(h)} - 1S_{(e)}$) for the four different samples under investigation as a function of CdS shell thickness. The HRTEM verified shell thicknesses (open symbols) are plotted along with the expected shell thicknesses (solid symbols). The dotted lines are fits of the HRTEM verified data to high order polynomials and act only as a guide to the eye. The area inside the gray box corresponds to the shifts associated with making the particles Cd-rich preceding shell growth (assuming 0.17 nm increase in radial shell thickness). It was found that the shifts associated with making the particles Cd-rich was not predictable and varied randomly with core size as well as between different batches of cores. Saturating the particle surface with cadmium prior to shell deposition allowed precise measurements of the optical changes as a function of shell thickness to be made beginning from particles with similar surface chemistries. Thus we assume that the first true CdS monolayer is present only after equimolar amounts of cadmium and sulfur have been added, subsequent to presaturating the surface with cadmium.

(26) Qu, L.; Yu, W. W.; Peng, X. *Nano Lett.* **2004**, *4*, 465.
(27) Klimov, V.; Bolivar, P. H.; Kurz, H. *Phys. Rev. B* **1995**, *52*, 4728.

The data of Figure 7A reveal two important trends. First, for shell coverages below approximately 1.2 nm (3 MLs), the energy loss per nanometre of CdS shell increases dramatically as the initial core size is decreased. As the shell coverage on all samples is further increased the energy shift of the first excited state begins to plateau. At shell coverages between 1.5 nm (4 MLs) and 2.19 nm (6 MLs) the energy loss of all the samples is below 4 meV. Second, as the initial core size decreases the *total* energy loss (after the growth of a 6 ML shell) increases dramatically. Although the first excited state energies of the initial core samples span approximately 431 meV, these energies condensed to span a range of only around 163 meV after 6 ML of CdS shell had been deposited (see Table 2). As a consequence preservation of emission color in CdSe/CdS heterostructures is impossible to achieve. For example, cores that have initial emission maxima around 515 nm shift to approximately 595 nm at the conclusion of shell growth. It is important to note here that in order to better preserve the core emission color zinc sulfide (ZnS) shells are required. The large band offsets between CdSe and ZnS strongly confine the exciton and as such only minimal energy losses are observed upon ZnS shell growth (see Supporting Information for a detailed analysis of CdSe/CdS/ZnS core/shell/shell nanocrystals). The inset of Figure 7A is a plot of the energy difference between the first and second excitonic transitions in 3.40, 3.84 and 4.68 nm CdSe cores as a function of increasing shell thickness. Data for 2.55 nm CdSe cores was not included due to the inability to resolve the higher order transitions in CdSe/CdS heterostructures with such small cores. Upon inspection we see that, for a given core size, CdS shell deposition has no effect on the energy difference between these two transitions. This implies that both s-type states couple into the shell with similar efficiency.

Given that the energy losses which occur upon the growth of the 6th ML are less than ~2 meV for all samples investigated here, we may assume the energy loss upon continued growth of the shell to be negligible. This allows for the determination of the total energy shift, $\Delta E_{tot}$, as a function of the initial energy of the core. The values obtained are as follows: 353 meV for a 2.55 nm core and 182 meV, 130 and 85 meV for 3.40, 3.84 and 4.68 nm cores respectively. Figure 7B displays a plot of $\Delta E_{tot}$ as a function of the initial energy of the core. The solid circles are those obtained for the four samples under investigation. The energy for the bulk band gap of CdSe (1.74 eV) is also plotted at $\Delta E_{tot} = 0$. This point may be considered a reference point given that no further changes to the absorbance spectra of semiconductor nanocrystals are expected once a particle reaches its bulk size. The data fit well to a straight line with an intercept at 1.92 eV (solid line), which implies that no shifts may be observed at room temperature for cores with energies (diameters) below ~1.92 eV (7.5 nm). To verify this fit, $\Delta E_{tot}$ for other initial core sizes are also plotted (solid triangles). These points were gathered from syntheses accomplished using the same synthetic method but without verification of shell thickness from HRTEM investigations. It is seen that these values agree well with those predicted from the fit. The evaluated empirical relation from the linear fit is as follows:

$$\Delta E_{(tot)} = 0.629E_{(core)} - 1.206E_{(core)} \in (1.92, 2.50) \quad (1)$$

This relation allows for quick determination of the total energy loss (in eV) simply by inputting the energy of the CdSe core (eV). Additionally, the high accuracy and wide range of the data collected on CdSe/CdS nanocrystals enables the generation of a contour plot, which correlates the CdSe core size, CdS shell thickness and energy of the first absorption maximum ($\lambda_{max}$). The contour plot is provided in the Supporting Information. The contour plot permits accurate determination of the CdS shell thickness (±0.1nm) simply from a knowledge of the $\lambda_{max}$ of the initial CdSe cores and the current $\lambda_{max}$ of the CdSe/CdS core/shells. It is important to note that the data are valid only for core sizes with first absorption maxima between 500 and 605 nm (2.48−2.05 eV) and shell thicknesses between 0 and 2 nm.

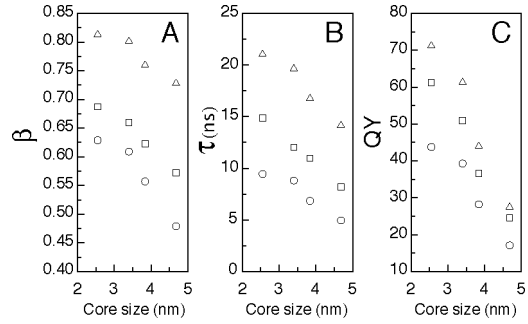


***Figure 8.*** Statistics from the stretched exponential fits to lifetime measurements obtained from *Samples 1−4* (6 ML CdS shell) in the as-prepared (□), trioctylphosphine/octadecylamine activated (△) and octane thiol quenched (○) states (A and B). The corresponding quantum yields in each of these states are also plotted (C).

**Lifetimes and Quantum Yield.** Given the large and varying extents to which the wave functions delocalize upon shell deposition it is important to establish how well a CdS shell electronically isolates the core from its environment. In order to test this, the lifetimes and QY of the core/shells were measured under various environmental conditions. Aliquots of the washed core/shells (*Samples 1−4* in ODE) were divided into three subsets. To create either *activating* or *quenching* environments, 10 $\mu$L of trioctylphosphine (TOP) and octadecylamine (ODA)[1] or octanethiol[1] were added to the samples respectively. As a reference, washed samples in ODE were also included in the analysis. The samples were heated at 60 °C for 6 h, then left at room temperature for approximately 20 h to ensure adequate time for ligand exchange. At this time aliquots of the samples were diluted with chloroform to obtain an absorbance of 0.1 at 400 nm (excitation wavelength) for the lifetime measurements and 0.05 at the appropriate excitation wavelengths for Rhodamine B (514 nm) and Rhodamine 6G (488 nm) to accurately determine the QY of the nanocrystals. The average of these two values were taken to be the QY of the particles.

The measured lifetimes were fitted to stretched exponentials of the form $A\exp(-t/\bar{\tau})^{\beta}$. These fits yield the average lifetime $\bar{\tau}$, and a beta ($\beta$) parameter ranging between 0 and 1. A $\beta$ value of 1 indicates a single exponential process, with decreasing values indicative of a broader distribution (increased number) of recombination pathways, provided by either defects inside the nanocrystal or by traps at the nanocrystal surface.[28]

Figure 8 shows plots of the values obtained for $\beta$ and $\bar{\tau}$ as well as the QY for *Samples 1−4* (6 ML CdS) in the as-prepared (squares), activated (triangles) and quenched (circles) states as a function of initial core size. We will now discuss each of these

(28) Gomez, D. E.; van Embden, J. L.; Jasieniak, J.; Smith, T. A.; Mulvaney, P. *Small* **2006**, *2*, 204.

parameters in turn. The first point to note is that the $\beta$ values (open squares -Panel A) obtained for the as-prepared samples decrease as the initial size of the nanocrystal cores increases. As mentioned above decreasing $\beta$ values in larger structures (assuming similar surface chemistries) are typical of an increasing number of surface sites, which may provide alternative recombination pathways. Interestingly, dramatic changes to $\beta$ are seen to occur upon both activation and quenching. These data immediately tell us that the recombination dynamics remain sensitive to the surface chemistry. This proves that at least one of the charge carriers still has access to the nanocrystal surface despite the thick potential barrier created by the ~2.2 nm thick CdS shell. The QY data (Panel C) support this conclusion. It is seen that the QY changes in dependence upon the nature of the surface bound ligands with fluctuations typically around 20%. The data of Panel C also reveals that CdSe/CdS heterostructures with smaller cores have an increased sensitivity to surface bound adsorbates. This observation is consistent with the expectation that excitons generated in core/shell nanocrystals with small cores spend more time close to the surface.[15]

Analysis of Panel B reveals that $\bar{\tau}$ decreases with increasing core size. Furthermore, this trend is maintained regardless of the ligands present at the NC surface. Explanation of this trend must therefore involve processes that are largely independent of the NC surface. In CdSe cores it is commonly observed that the band-edge lifetime increases weakly with core size.[29] This has been attributed to decreased confinement within the nanocrystal, which reduces the interaction of the charge carriers in the excited state and thus lengthens the band-edge lifetime.[30] Effective mass calculations of CdSe/CdS heterostructures attribute the reduction to confinement upon shell deposition to efficient delocalization of the lighter electron across the particle with the hole remaining mainly confined to the core.[15] Recalling that smaller cores exhibit greater $\Delta E_{tot}$ values (increased electron delocalization) we expect more efficient charge separation to occur in CdSe/CdS heterostructures with smaller cores. We therefore attribute the observed increase of the lifetime with decreasing core size to more efficient charge separation and reduced Coulomb attraction between the charge carriers in the excited state.

The recombination dynamics were also measured as a function of shell thickness. Figure 9A shows a series of lifetime traces taken after each subsequent layer of CdS shell growth on an intermediate size core (3.40 nm). Panels B and C are plots of the $\beta$ and $\bar{\tau}$ values obtained from fitting the lifetimes. We see that upon making the particles Cd-rich both $\beta$ and $\bar{\tau}$ increase dramatically. The injection of cadmium saturates the surface selenium atoms. The newly formed Cd-rich surface is subsequently passivated by the metal binding ligands present in the growth solvent, resulting in a more favorable surface chemistry for the particle.[16] This result is expected given that there are no chalcogen binding ligands present to passivate surface selenium atoms. Upon deposition of the first ML of CdS another sharp increase in $\beta$ is observed, indicative of epitaxial surface passivation and increased electronic isolation of the core from its environment. Upon continued shell growth an increase in both $\beta$ and $\bar{\tau}$ is observed until the CdS shell thickness reached 3 ML, at which point continued shell growth resulted in a decrease in both parameters. The reversal of the initial trends

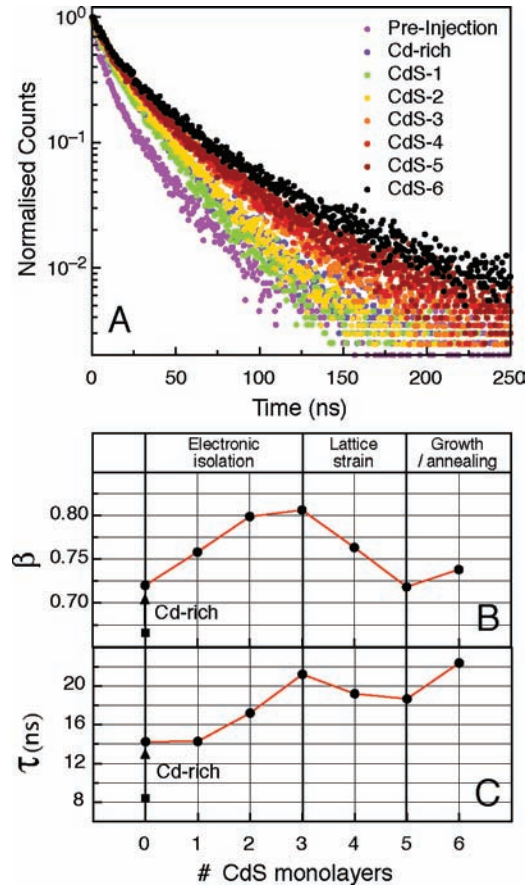


***Figure 9.*** (A) Lifetime traces as a function of CdS shell growth. (B) and (C) $\beta$ and $\bar{\tau}$ values obtained from the stretched exponential fits of these lifetime traces, respectively.

observed for $\beta$ and $\bar{\tau}$ may be attributed to increased lattice strain within the structure. The induced strain is typically relieved by the creation of defects in the lattice, which act as nonradiative recombination centers for the charge carriers. As the data for the sixth ML was recorded from an aliquot taken at the end of the reaction, the increase in both parameters observed after the deposition of the final monolayer is likely due to the annealing of the nanocrystals *after* the termination of shell growth.

## Concluding Remarks

In this paper we have reported a reliable synthetic technique to grow thick wurtzite CdS shells on a wide range of CdSe core sizes with monolayer control of shell thickness. Most importantly, we have verified the shell thicknesses (and core diameters) through the use of HRTEM investigations, adding much needed validity to the observed changes in optical properties. We have for the first time obtained reliable transition energies as a function of *both* core size and shell thickness. These data enabled the generation of a calibration plot, which allows for easy determination of CdS shell thickness over a wide range of core sizes circumventing the need for time-consuming HRTEM analyses. We expect that these data will also aid in the development of more accurate quantum mechanical models used to describe CdSe/CdS heterostructures. *In-situ* measurements have revealed that sulfur growth is approximately an order of magnitude faster than cadmium growth, which we attributed to the absence of strong S-binding additives in the growth medium. Lifetime and QY measurements have prove that in spite of the ~2.2 nm thick CdS shell, one or both of the charge carriers still has access to the particle surface.

(29) Schlegel, G.; Bohnenberger, J.; Potapova, I.; Mews, A. *Phys. Rev. Lett.* **2002**, *88*, 137401.
(30) Garrett, M. D.; Bowers, M. J.; McBride, J. R.; Orndorff, R. L.; Pennycook, S. J.; Rosenthal, S. J. *J. Phys. Chem. C* **2008**, *112*, 436.

**Acknowledgment.** J.v.E. and J.J. acknowledge support through an APA scholarship. P.M. thanks the ARC and the University of Melbourne for support through the Federation Fellowship program.

**Supporting Information Available:** Contour plots for the determination of CdS shell thickness, HRTEM images of CdSe/CdS NCs synthesized using either cadmium oleate or Cd-TMPPA and data on CdSe/CdS/ZnS multishell NCs. This material is available free of charge via the Internet at http://pubs.acs.org.

JA9030209